Eur. Phys. J. D (2021) 75:230
https://doi.org/10.1140/epjd/s10053-021-00246-w

THE EUROPEAN PHYSICAL JOURNAL D

Regular Article – Atomic and Molecular Collisions

# Dissociative attachment of low-energy electrons to acetonitrile

Thomas F. M. Luxford[1], Jaroslav Kočišek[1], Lukas Tiefenthaler[2], and Pamir Nag[1,a]

[1] J. Heyrovský Institute of Physical Chemistry, Czech Academy of Sciences, Dolejškova 3, 18223 Prague, Czech Republic
[2] Institut für Ionenphysik und Angewandte Physik Universität Innsbruck, Technikerstraße 25, 6020 Innsbruck, Austria

Received 26 June 2021 / Accepted 12 August 2021 / Published online 24 August 2021


**Abstract.** We experimentally probed the low-energy electron-induced dissociation of acetonitrile and acetonitrile-$d_3$ and performed density functional theory calculations to support the experimental results. The previous studies on electron attachment to acetonitrile presented a number of contradictory findings, which we aimed to resolve in the present study. We observed the formation of $H^-$, $CH_2^-$, $CH_3^-$, $CN^-$, $CCN^-$, $CHCN^-$ and $CH_2CN^-$ anions and the corresponding deuterated fragments for acetonitrile-$d_3$ by dissociative electron attachment, and measured ion yields curves of each fragment. We saw no evidence for associative electron attachment to form the parent ion in these measurements. We also have measured the kinetic energy and angular distribution of selected fragments using a velocity map imaging (VMI) spectrometer.

## 1 Introduction

Acetonitrile, $CH_3CN$, is an important astrophysical molecule, which has been directly observed in molecular clouds [1,2] and in Titan's atmosphere [3]. Furthermore, the $CN^-$ anion is one of the most abundant molecular anions detected in Titan's atmosphere [4], and low-energy electron-induced dissociation of acetonitrile might be an important source of $CN^-$ ions. Acetonitrile is believed to have been an important source of nitrogen in prebiotic chemistry [5].

When ionizing radiation (such as high energy electrons or $\beta$ particles, $x$-rays, $\gamma$ rays or any other cosmic radiation) interacts with a bulk medium, such as interstellar molecular clouds or biological tissue, a large number of low-energy electrons are produced. These low-energy electrons play an important role in molecular fragmentation. When a low-energy electron (up to around 15 eV) interacts with a molecule, the electron may get captured to form a temporary negative ion (TNI). The TNI can subsequently dissociate into an anionic and neutral fragment, in a process known as dissociative electron attachment (DEA). Over the last several decades, DEA has been studied in reference to processes in interstellar medium, in atmospheres [6–8] and in biology [9–11].

Several experimental and theoretical studies on electron collision with acetonitrile have already been conducted. Hitchcock *et al.* [12] and Jordan and Burrow [13] performed electron transmission spectroscopy studies of acetonitrile to determine the resonance energies. Hitchcock et al. observed a $\pi^*$ resonance at 2.82 eV and two weak features, which they assigned to be $\sigma^*$ resonances at 5.7 and 6.8 eV. Jordan and Burrow also observed the $\pi^*$ resonance at 2.84 eV and a broad resonance around 6-eV. Edard et al. [14] studied the vibrational excitation via $\pi^*$ and $\sigma^*$ state, and Gochel-Dupuis et al. [15] had performed the electron energy loss study of acetonitrile with a higher incident electron energy to probe the outer shell excitation.

Fujimoto et al. [16] performed R-matrix calculations to study low-energy (1–10 eV) electron scattering from acetonitrile. The authors included the polarization effect into the calculation and observed three resonances, a $\pi^*$ resonance at 2.7 eV, a broad resonance around 6.59 eV and a narrow resonance around 9.66 eV. The resonance around 6 eV was considered to be a $\sigma^*$ shape resonance, whereas the high-lying resonance at 9.66 eV to be a Feshbach resonance. Gutsev et al. [17] calculated the structure of acetonitrile and the parent negative ion state, $CH_3CN^-$ and estimated the electron affinity of $CH_3CN$ using three different ways.

Dissociation of acetonitrile and subsequent formation of different anionic fragments due to interaction with a range of atomic projectiles and charge transfer reactions have also been studied by several research groups in past [18–20]. Heni and Illenberger [21] and Sailer et al. [22] have studied the DEA of acetonitrile and observed the $CH_2CN^-$, $CHCN^-$, $CCN^-$, $CN^-$ and $CH_3^-$ anionic fragments. The authors were not able to observe the parent negative ion. The electron-induced reaction in condensed films of $CD_3CN$ [23] and acetonitrile [24] was performed using thermal desorption spectrometry. The

[a] e-mail: pamir.nag@jh-inst.cas.cz (corresponding author)

authors studied the ion yields of $H^-$, $CH_2^-$, $CH_3^-$ and $CN^-$ anions, and also observed the weaker presence of $CH^-$, $CHCN^-$ and $CH_2CN^-$ ions. The authors noted that the presence of $CH_2^-$ is particularly striking, since the ion was not observed in the previous gas-phase studies [21,22].

An interesting open question is the stability of acetonitrile parent anion. Uncertainty surrounding the parent ion arises due to the fact that an ion with a mass of 41 Da can either be $CH_3CN^-$, or the $^{13}C$ isotopologue of $CH_2CN^-$. In an earlier report, Stockdale et al. [20] observed the stable $CH_3CN^-$ ion in the collision of acetonitrile with Ar atoms in a highly excited Rydberg state. The authors also observed the production of mass 41 Da ($CH_3CN^-$ anion) due to low-energy electron interactions with a peak around 4 eV. Sugiura and Arakawa [25] observed the formation of $CH_3CN^-$ anions by the charge transfer reaction from Rydberg states of rare gases using a time of flight mass spectrometer. Later, Klots [26] repeated the experiment using deuterated acetonitrile and observed $CD_3CN^-$ in the bimolecular reaction: $CD_3CN^* + CD_3CN \rightarrow CD_3CN^- + CD_3CN^*$. Thus, unambiguously concluded that the observation of acetonitrile parent negative ion is not an artefact arising from $CH_2CN^-$ ion with one $^{13}C$ isotope.

The mass 41 Da anion was also observed in electron collisions with acetonitrile clusters by Hashemi and Illenberger [27], with peaks around 3 eV and 8.5 eV incident electron energies. The authors concluded that the peak around 3 eV arose from $CH_2CN^-$ with one $^{13}C$ atom, while the peak around 8.5 eV is from $CH_3CN^-$. Tsuda et al. [28] observed the parent negative ions for 80 and 40 eV electron interaction with the acetonitrile, whereas for 9.5 eV incident electron energy $CH_3CN^-$ had not been observed. No evidence of $CH_3CN^-$ anion formation was also observed by Warmack et al. [19] in collisional ionization of acetonitrile with atomic caesium and potassium. The $CH_3CN^-$ anion was not observed in any of the previous low-energy electron collision studies with isolated gas phased acetonitrile molecule [21,22]. All this implies that $CH_3CN^-$ is not formed in collisions with free electrons, or its lifetime with respect to autodetachment and DEA is extremely short.

In a recent study, Li et al. [29] measured the ion yield curves of $CHCN^-$, $CH_2CN^-$ and $CN^-$ anions produced by DEA to acetonitrile and also measured the kinetic energy and angular distribution of $CN^-$ fragments using a VMI spectrometer. The authors observed ion yield curves significantly different from the previous reports [20–22].

While electron attachment to acetonitrile has been studied by different research groups, both experimentally and theoretically, a number of questions remain unanswered. The $CH_2^-$ ion was observed in the condensed phase but not in the gas phase. Associative electron attachment to form the parent ion has not been conclusively observed experimentally. $H^-$ anion production is energetically possible and one would expect to observe it, but none of the previous studies reported the ion yield curve of the $H^-$ fragment. The different experimental studies have produced significantly different ion yield curves. No data on the kinetic energy distribution or angular distribution of the fragment anions, except a single report of only $CN^-$ fragment [29], are available in the literature. To address all these issues, we re-investigated DEA to acetonitrile by performing complimentary experiments on three independent setups.

## 2 Experiment

Three experimental setups were used for the present study to perform complementary experiments. A brief description of the each setup is presented below:

(A) The TEM–QMS (trochoidal electron monochromator–quadrupole mass spectrometer) setup [30,31] was used to study the anionic fragments produced by dissociative electron attachment (DEA) to $CH_3CN$ and to measure the ion production efficiency of each fragment as a function of the incident electron energy (ion yield curve). The TEM–QMS setup was originally constructed and operated at the University of Fribourg, Switzerland [32], and then transported to Prague and modified [33]. In brief, a continuous electron beam was produced by a tungsten cathode and the distribution of electron energies was narrowed by a trochoidal electron monochromator. The electron beam was crossed with an effusive molecular beam containing the target molecule. Electrostatic lenses direct any formed anions toward a quadrupole mass filter, which selects anions with a single mass-to-charge ratio to be detected using a channeltron. Ion yield curves were recorded by varying the electron energy and measuring the yield at a particular mass. In these measurements, the resolution of the incident electron beam was around 100 meV. The mass resolution of the quadrupole was around 100 ($M/\Delta M$), as a result, ions that are separated by 1 Da cannot always be completely isolated, especially when one peak is much more intense than the other.

(B) The CLUB (CLUster Beam) experimental setup has also been used to study the anions formed due to DEA with the $CH_3CN$ molecule. The experimental setup has been described in detail in previous papers [34,35], so only a short overview will be given here. While the apparatus is typically used for molecular beam studies, the setup also allows the study of isolated gas phase molecules by introducing them as a background gas into the time of flight (TOF) chamber [36,37]. Acetonitrile was introduced into the vacuum chamber of the TOF mass spectrometer (base pressure $1 \times 10^{-8}$ mbar) to reach the pressures around $4 \times 10^{-7}$ mbar sufficient for the measurement. In the reaction region of the TOF, the molecules were exposed to low-energy electrons produced from a simple magnetically collimated electron gun based on a heated tungsten filament.

Product anions were extracted from the interaction region into a reflectron time of flight mass spectrometer. Mass spectra were recorded for electron energies 0.6-10.6 eV in steps of 0.25 eV. Compared to the TEM-QMS setup, the CLUB setup has an excellent mass resolution of up to $M/\Delta M = 4000$, but the setup has a simple electron gun not suitable for electron attachment spectroscopy studies [38].

(C) A velocity map imaging (VMI) spectrometer combined with a trochoidal electron monochromator [7,39] was also used for the current report to measure the angular distribution and kinetic energy of the anionic fragments. The VMI setup is based on a trochoidal electron spectrometer originally built and operated at the University of Fribourg, Switzerland [40,41], and then transferred to Prague. The setup has undergone several modifications with time, and details of the VMI spectrometer used for the present study can be found in an earlier report [7]. In brief, a pulsed electron beam with 40-kHz repetition rate and of 200-ns width was produced using a trochoidal electron monochromator. The electron beam interacts perpendicularly with an effusive molecular beam in a field free condition at the interaction region of the VMI spectrometer. The produced anions are pulsed extracted from the interaction region and are recorded using a time and position sensitive detector with 40-mm active diameter. The extraction pulse was applied around 100-ns after the electron beam pulse. The angular distribution of the anionic fragments was obtained from the central time sliced images, whereas the half-'Newton sphere' was used to measure the kinetic energy distribution [7]. The setup is also capable of measuring ion yield spectra. The mass resolution is lowered due to the VMI requirements, but it can still resolve the central part of the Newton spheres of two adjacent masses with 1-Da mass difference around the 40-Da mass.

From energy and momentum conservation, it is possible to calculate the appearance energy and kinetic energy of an anionic fragment produced via DEA process expressed as:

$$e^- + M \rightarrow (M^-)^* \rightarrow X^- + Y^* \tag{1}$$

The appearance energy of an anionic fragment, $X^-$, can be expressed as:

$$E_{th}(X^-) = D_{bond} - EA(X) + E^*(Y) \tag{2}$$

where $D_{bond}$ is the bond dissociation energy. It is possible to have more than one neutral fragment, in which case $D_{bond}$ represents sum of all the bond dissociation energies. $EA(X)$ is electron affinity of the fragment $X$ and $E^*(Y)$ is the excitation energy of the neutral fragment, $Y$. The kinetic energy ($E_{ke}$) of the fragment negative ion, $X^-$, can be expressed as:

$$E_{ke} = \left(1 - \frac{m}{M}\right) \times \left[E_{in} - E_{th}(X^-)\right] \tag{3}$$

where $m$ and $M$ are the masses of the anionic fragment and the parent molecule, respectively.

To measure the kinetic energy distribution of the anionic fragment, we have calibrated the spectrometer using the kinetic energy distribution of $O^-$ ions created via DEA of $CO_2$ at the 8.2-eV resonance [42]. Current experiments were performed at around 1.0 to 3.0 $\times 10^{-6}$ mbar background pressure, and to record the VMI images, each set of data were measured for around 30 to 40 hours depending on the statistics. To ensure that the incident electron energy did not shift during the long measurements or due to presence of acetonitrile in the chamber, the VMI data acquisitions were paused from to time and the energy calibration was checked by letting $CO_2$ into the chamber in the presence of acetonitrile and measuring the $O^-/CO_2$ production around the 4.4-eV resonance. The presence of energy shift, if any, with less than 250 meV was corrected, and the VMI measurements were continued after removing the $CO_2$ from the chamber. If the energy scale was found to be shifted by more than 250 meV, then the data set was discarded. The incident electron beam energy scale of all three experiments was calibrated using the 4.4-eV resonance peak [43,44] of the $O^-$ production from $CO_2$.

### The molecular samples

The experiments with $CH_3CN$ were performed using 99.8% pure anhydrous acetonitrile sample, whereas the experiments with $CD_3CN$ were performed using $\geq$ 99 % pure assay having $\geq$ 99.8 atom % D. Both of the samples were commercially purchased from Sigma-Aldrich. During the experiment, the liquid sample was kept in a heat bath at 22°C constant temperature providing enough vapour pressure for the present gas phase study.

## 3 Threshold energy calculations

To support the experimental results, we calculated threshold energies for different DEA reaction pathways at the B3LYP/aug-cc-pVTZ level of theory using the Gaussian 16 software [45]. Geometry optimisations and single point energy calculations were performed for the acetonitrile molecule and all possible anion and neutral dissociation products. From the single point energies, threshold energy values were obtained using the formula:

$$E_{th} = E_{M_a^-} + E_{M_b} - E_M \tag{4}$$

where $E_{M_a^-}$ and $E_{M_b}$ are the sum of electronic and zero-point energies of the anion and neutral fragments, respectively (if there are multiple neutral fragments, then $E_{M_b}$ is the sum of all electronic and zero-point energies of all neutral fragments), and $E_M$ is the energy

of the parent acetonitrile molecule. This equation can be rearranged as

$$E_{th} = BDE - EA_{M_a} \quad (5)$$

where $BDE$ is the bond dissociation energy of the bond being broken (or the sum of all bonds being broken) and $EA_{M_a}$ is the electron affinity of the fragment $a$. This approach is well established and has been used in earlier reports [31,46].

## 4 Results and Discussion

The negative ion mass spectra and ion yield curves were independently measured using the TEM-QMS, CLUB and VMI spectrometer setups. As discussed in the experimental section, each of the instruments has a different mass and energy resolution as well as detection efficiency. The three independent measurements ensure that there are no systematic error in the measurements. The velocity map images of selected ion fragments were measured using the VMI setup.

### 4.1 Mass spectra

The energy-integrated mass spectrum of acetonitrile measured over 0.6–10.6 eV incident electron energy using the CLUB setup is shown in the top panel of Fig. 1. Similar to the previous reports of Heni and Illenberger [21] and Sailer *et al.* [22], we observed the $CH_3^-$, $CN^-$, $CCN^-$, $CHCN^-$ and $CH_2CN^-$ anionic fragments, in addition $CH_2^-$ and a specie with mass 41-Da. The $CH_2^-$ ion had been observed previously in the electron stimulated desorption of condensed acetonitrile, but not in the gas phase DEA studies [24].

The ions at mass 41-Da can either be the $CH_3CN^-$ parent ion (41.027 Da), or the $^{13}C$ isotopologue of $CH_2CN^-$ (41.022 Da). The stability of the acetonitrile parent anion is a matter of ongoing discussion as mentioned in the introduction. Formation of the parent negative ion state of acetonitrile was observed in clusters [27] but not for DEA to the isolated gas phase molecule. The critical dipole moment required to form a negative ion is $\geq$ 2.5-D [21,47,48]. In a theoretical study, Garrett [49] concluded that any molecule having dipole moment $\geq$ 4-D will form thermally stable negative ions. The dipole moment of $CH_3CN$ is $3.913 \pm 0.002$-D [50], which is considerably greater than the critical value. Acetonitrile does form a stable dipole-bound state with a positive vertical electron affinity of 11.5 meV, as measured experimentally by Desfrançois et al. [51] Gutsev et al. [17] calculated the structure of acetonitrile and its anion $CH_3CN^-$ and found that the $CH_3CN^-$ anions in addition to a dipole bound state also possess a valence state or 'normal bound state'. In the potential energy surface, the $CH_3CN^-$ state has a local minimum and is separated from the dissociation limit by 0.14 eV. Our calculated value of electron affinity is slightly negative

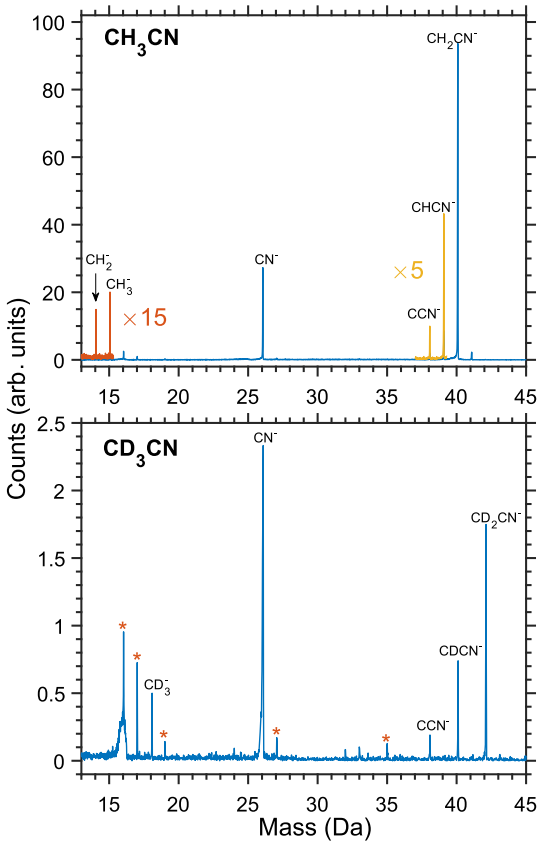


**Fig. 1** Cumulative mass spectra of acetonitrile and acetonitrile-$d_3$ integrated over the incident electron energy range 0.6–10.6 eV with step size 0.25 eV, measured using the CLUB experimental setup. The background peaks were marked using '*'

(-0.2 eV, see Table 1), which is understandable as we had employed only standard diffused orbital functionals (augmented basis sets) which are not sufficient to describe so weakly dipole-bound electrons.

To conclusively determine if low-energy electron attachment leads to parent negative ion formation in $CH_3CN$ or not, we repeated the experiment with the deuterium substituted molecule, acetonitrile-$d_3$, for which the mass spectrum is shown in the lower panel of Fig. 1. In the acetonitrile-$d_3$ mass spectrum, the parent ion (44-Da) is clearly not present, while the $^{13}C$ isotopologue of $CD_2CN^-$ (43-Da) is. The relative intensity of $CD_2CN^-$ and mass 43-Da for acetonitrile-$d_3$ is similar to that of the relative intensities between $CH_2CN^-$ and mass 41 Da for acetonitrile. From these observations, we see no evidence of long-lived parent ion formation for acetonitrile. Due to the presence of some electronic noise, it was not possible to reliably measure the presence of $H^-$ ions produce from the acetonitrile (and $D^-$ from the acetonitrile-$d_3$) using the CLUB setup.

While the same species are observed in the mass spectra for $CH_3CN$ and $CD_3CN$, the intensities are dramatically different between the two isotopologues. This is due to the longer dissociation timescale of $CD_3CN$,

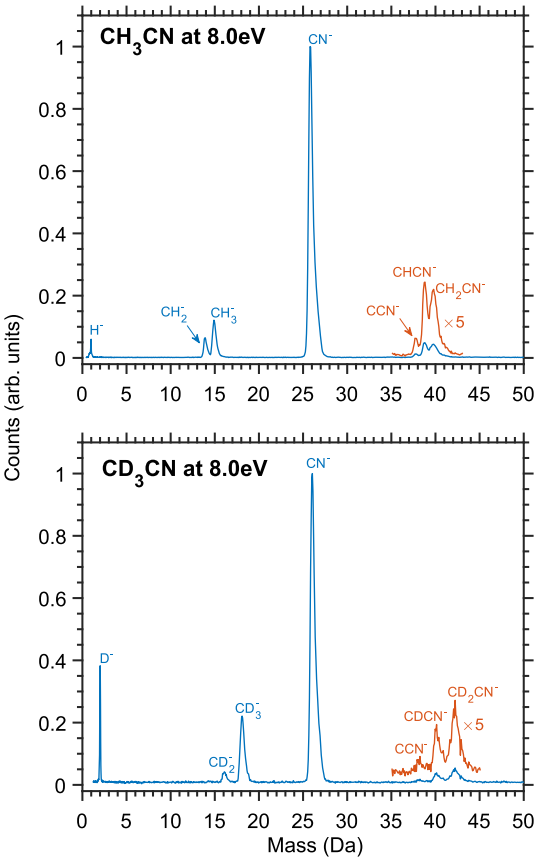


**Fig. 2** Mass spectra of the fragment anion produced due to DEA to $CH_3CN$ and $CD_3CN$ recorded using the VMI setup at 8.0 eV constant incident electron energy are shown on the top and bottom panels, respectively. The relative intensity of $H^-$ ions is not reliable as discussed in the text

caused by the mass difference of the H and D atoms. As DEA is in competition with electron autodetachment, a longer dissociation timescale will correspond to a lower DEA product ion yield [52].

Mass spectra for the fragment anions formed at constant incident electron energy of 8.0 eV, measured using the VMI spectrometer, are shown in Fig. 2. The mass resolution of the VMI setup is too low to completely separate out the weak 41-Da mass peak from the neighbouring $CH_2CN^-$ mass peak for acetonitrile, and mass 43-Da from $CD_2CN^-$ peak for acetonitrile-$d_3$, respectively. Otherwise, we were able to observe all the mass fragments produced from acetonitrile and acetonitrile-$d_3$ seen with the CLUB apparatus. In addition, we were able to observe the $H^-$ and $D^-$ ions using the VMI setup as a DEA product of acetonitrile and acetonitrile-$d_3$, respectively. Due to its lower mass and higher kinetic energy, it was not possible ensure total ion collection for the $H^-$ fragment using the VMI setup. Therefore, the relative intensity of $H^-$ with respect to other mass fragments is not reliable. Care was given to ensure that at 8 eV the $H^-$ ions are not produced from the background or residual substrate present in the gas line, whereas the presence of $D^-$ ions in Fig. 2 is more reliable, as due to higher mass we were able to collect most of the produced ions. Also, it is extremely unlikely for any deuterated substrate to be naturally present in background, so the $D^-$ ions can only be produced from the acetonitrile-$d_3$ sample.

### 4.2 Ion yield curves

The ion yield curves of $CH_2^-$, $CH_3^-$, $CN^-$, $CHCN^-$ and $CH_2CN^-$ and the corresponding deuterated fragments produced via DEA to acetonitrile and acetonitrile-$d_3$ were measured using the TEM-QMS setup from 0 to 10 eV and are shown in Fig. 3. Due to very low intensity, it was not possible to measure the ion yield curve of the $CCN^-$ fragment using this setup. The ion-yield curves of $D^-$ and $CCN^-$ fragments produced from acetonitrile-$d_3$ were measured using the VMI setup and are shown in Fig. 4a, b, respectively. To aid the interpretation of the experimental results, threshold energies of different fragmentation pathways for acetonitrile were calculated, which represent the minimum electron energy at which these processes become energetically accessible. The calculated threshold energies are listed in Table 1 and are shown as vertical lines in the left column of Fig. 3.

#### $H^-$ and $D^-$ production

It was not possible to measure the ion-yield curve of lighter masses, like $H^-$ and $D^-$ using the TEM-QMS setup. Also using the VMI setup it was not possible to ensure total ion collection for the $H^-$ fragment produced, as a result it was not possible to reliably measure the ion-yield curve of the $H^-$ fragment as well. However, we were able to measure the ion-yield curve of the $D^-$ fragment produced from acetonitrile-$d_3$ using the VMI setup, which is shown in Fig. 4a. The peak position and structure of $D^-$ are similar to the previous report of $H^-$ produced by an electron-induced reaction in condensed films of acetonitrile [24]. None of the previous gas phase DEA study on acetonitrile [20–22,29] reported the ion yield curve of $H^-$, possibly as a result of limitations of the mass spectrometers and the presence of background $H^-$. Based on the threshold energies in Table 1, simple C-H bond fragmentation to form $H^-$ is energetically accessible, and so is the most probable dissociation pathway.

#### $CH_2^-$ and $CD_2^-$ production

As shown in Fig. 3 for both $CH_2^-$ and $CD_2^-$, we observed a peak around 7.5 eV incident electron energy. The $CD_2^-$ peak is noticeably broader than that of $CH_2^-$. Threshold calculations (Table 1) show that $CH_2^-$ is formed together with an HCN neutral co-fragment, rather than separate H and CN co-fragments.

This is for the first time $CH_2^-$ anion production has been observed for DEA to acetonitrile. It was not observed in the studies of Heni and Illenberger [21] and

**Table 1** Potential fragmentation pathways of acetonitrile and the threshold energies calculated at B3LYP/aug-cc-pVTZ level of theory

| m/z | Anion | Neutral products | $E_{th}$ (eV) |
|---|---|---|---|
| 41 | $CH_3CN^-$ | | 0.20 |
| 40 | $CH_2CN^-$ | H | 2.37 |
| 39 | $CHCN^-$ | $H_2$ | 1.78 |
| | $CHCN^-$ | 2H | 6.29 |
| 38 | $CCN^-$ (t) | $H_2$ + H | 5.28 |
| | $CCN^-$ (s) | $H_2$ + H | 6.35 |
| | $CCN^-$ (t) | 3H | 9.78 |
| | $CCN^-$ (s) | 3H | 10.85 |
| 26 | $CN^-$ | $CH_3$ | 1.17 |
| | $CN^-$ | CH (d) + $H_2$ | 5.76 |
| | $CN^-$ | $CH_2$ (t) + H | 5.93 |
| | $CN^-$ | $CH_2$ (s) + H | 6.41 |
| | $CN^-$ | CH (q) + $H_2$ | 6.69 |
| | $CN^-$ | CH (d) + 2H | 10.27 |
| | $CN^-$ | CH (q) + 2H | 11.20 |
| | $CN^-$ | C + $H_2$ + H | 13.98 |
| | $CN^-$ | C + 3H | 18.49 |
| 15 | $CH_3^-$ | CN | 5.10 |
| | $CH_3^-$ | C + N | 17.42 |
| 14 | $CH_2^-$ | HCN | 3.69 |
| | $CH_2^-$ | CN + H | 9.19 |
| 1 | $H^-$ | $CH_2CN$ | 3.04 |
| | $H^-$ | CCN(d) + $H_2$ | 7.29 |
| | $H^-$ | CHCN(t) + H | 7.38 |
| | $H^-$ | CHCN(s) + H | 8.06 |
| | $H^-$ | CCN(q) + $H_2$ | 8.39 |
| | $H^-$ | $CH_2$(t) + CN | 9.07 |
| | $H^-$ | $CH_2$(s) + CN | 9.55 |
| | $H^-$ | CCN(d) + 2H | 11.79 |
| | $H^-$ | CCN(q) + 2H | 12.89 |
| | $H^-$ | CH(d) + H + CN | 13.40 |
| | $H^-$ | CH(q) + H + CN | 14.33 |
| | $H^-$ | C + $H_2$ + CN | 17.12 |
| | $H^-$ | C + 2H + CN | 21.62 |

The (s), (d), (t) and (q) denote singlet, doublet, triplet and quadruplet states, respectively

Sailer et al. [22]. It is possible that this peak was overlooked in the previous studies, due to a combination of its low intensity (around 25 times lower than the most intense product), and the mass-to-charge ratio = 16, which overlaps with the common background $O^-$. The similar shape of $CH_2^-$ and $CD_2^-$ ion yield curves in the present experiment unambiguously demonstrate the $CH_2^-$ formation. The $CH_2^-$ ions were also observed for the electron-induced reaction in condensed films of acetonitrile by Bass et al., [24] for which the ion yield started from around 6 eV. This is similar to the present gas phase study, but with a broader peak.

## $CH_3^-$ and $CD_3^-$ production

For both $CH_3^-$ and $CD_3^-$ anions, we observed a peak around 7.5 eV incident electron energy. This is consistent with the previous studies Heni and Illenberger [21] and Sailer et al. [22], who also observed the $CH_3^-$ ions around the same energy range. The threshold calculations suggest that $CH_3^-$ produced with a CN co-fragment.

## $CN^-$ production

The ion yield curves of $CN^-$ produced from acetonitrile and acetonitrile-$d_3$, measured using the TEM-QMS setup, are shown in Fig. 3. The $CN^-$ ion yield curves for both acetonitrile and acetonitrile-$d_3$ contain two peaks, a smaller one at around 3.5 eV and a larger peak around 8 eV. In most of the previous studies [21,22,29], the higher energy peak of $CN^-$ was observed around 8-eV, which is consistent with our observation. On the other hand, Stokedale et al. [20] observed it around 8.5 eV. Heni and Illenberger and Stokedale et al. reported the lower energy peak at around 3.5-eV similar to the present report, whereas Sailer et al. and Li et al. [29] observed it around 2-eV. The threshold

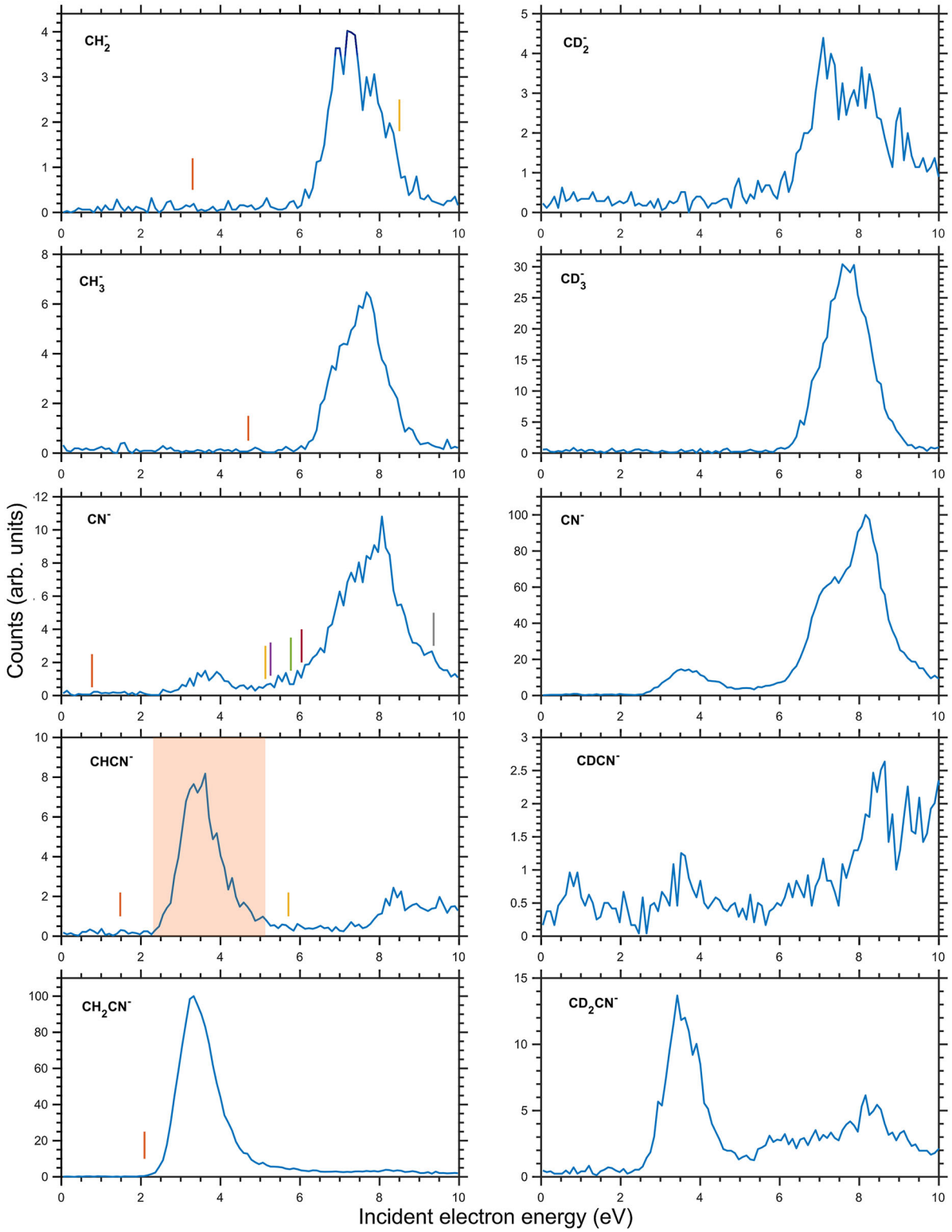


**Fig. 3** Ion yield curves of five different fragments, as indicated on each graph, produced due to DEA to acetonitrile are shown on the left column and the similar fragments produced due to DEA to acetonitrile-$d_3$ are shown on the right column. The calculated threshold energy values for different dissociation channels (as listed in Table 1) for each of the fragment produced from acetonitrile are shown using the small vertical bars on each graphs on the left column. For $CHCN^-$ ions, the strong peak around 3.5 eV is an experimental artefact arising due to the strong neighbouring $CH_2CN^-$ peak. This region is marked using the red shadow and discussed in detail in text. Note: the counts are in arb. units and the relative intensities of any particular fragment produced from acetonitrile and its corresponding fragment from acetonitrile-$d_3$ are not scaled

calculations show that simple C-C bond cleavage of the parent ion accounts for both peaks in the ion yield of $CN^-$. At around 8.5 eV, the energy is sufficient to allow further fragmentation of the neutral $CH_3$ co-fragment.

### $CCN^-$ production

As discussed earlier, due low intensity, it was not possible to satisfactorily measure the ion yield curve of $CCN^-$ using the TEM-QMS setup. The ion yield of $CCN^-$ produced from the acetonitrile-$d_3$ was measured using the VMI setup and is shown in Fig. 4b. The ion yield curve of $CCN^-$ shows one peak around 8.5 eV, similar to previous reports [21,22].

### $CHCN^-$ and $CDCN^-$ production

The ion yield curves of $CHCN^-$ and $CDCN^-$ measured using the TEM-QMS setup are shown in Fig. 3. The ion yield of $CDCN^-$ contains a smaller peak at about 4.0 eV, and a larger peak with an onset at about 8.0 eV. This is similar to the previous reports of Heni and Illenberger [21], and Sailer et al. [22]. The ion yield curve for $CHCN^-$ (mass 39 Da) measured using the TEM-QMS setup contains a more intense peak at 3.5 eV, which is an experimental artefact, arising from the neighbouring $CH_2CN^-$ (mass 40 Da) ion signal due to the limited mass resolution of the apparatus. This artefact is only observed due to the large difference in intensities of the two ions ($CH_2CN^-$ is about an order of magnitude more intense than $CHCN^-$), and similar artefacts are not observed for other neighbouring ions.

$CHCN^-$ is formed by the loss of two H atoms from the parent ion, which can dissociate separately, or as a single $H_2$ molecule. The threshold energy for loss of $H_2$ corresponds to the onset of the lower-energy peak, while the threshold energy for loss of two H atoms lies between the two peaks. This means that for the 3.5 eV peak the ions are produced entirely by the loss of $H_2$, while the ions in the 8.5 eV peak might arise from either mechanism or a combination of the two.

### $CH_2CN^-$ and $CD_2CN^-$ production

The $CH_2CN^-$ ion yield shows a single peak at around 3.5 eV, consistent with the report of Sailer et al. [22], and a structure in the higher energy range between 6–10 eV reported also by Heni and Illenberger [21]. For $CD_2CN^-$, the same peaks are present, but the relative intensity of the higher energy peak is much greater.

This difference is caused by the different dissociation timescales between the two isotopologues, similar to the differences in relative intensity observed between the different DEA products described above [52]. Deuterium substitution significantly prolongs the dissociation time, for which autodetachment is possible. The change of relative intensity indicates that autodetachment is very effective and further supports our conclusion that the anion state of $CH_3CN$ is only weakly bound, with lifetime not enough to be detected using the experimental setups used.

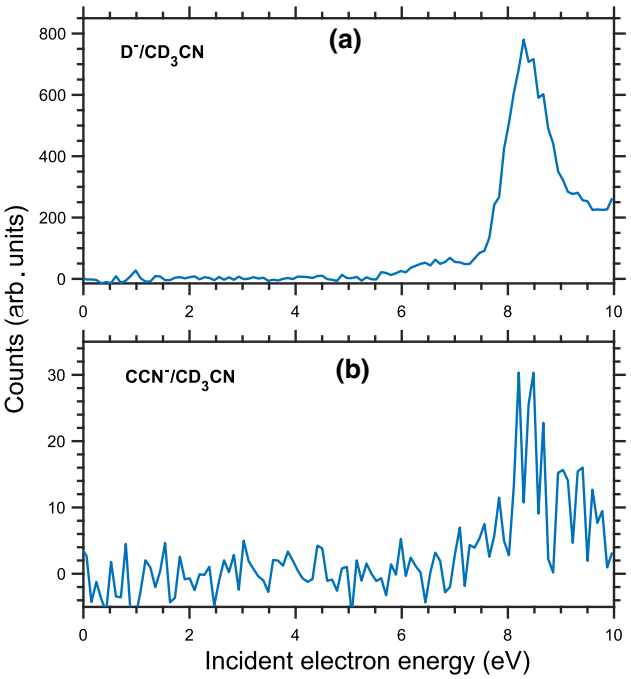


**Fig. 4** The ion yield curves of $D^-$ and $CCN^-$ fragments produced due to DEA to acetonitrile-$d_3$ measured using the VMI setup are shown in (**a**) and (**b**), respectively

### 4.3 Velocity map images

The velocity map imaging experiment was only performed with non-deuterated acetonitrile. The VMI images were taken at incident electron energies of 3.3, 3.6, 3.9, 8.0 and 8.3 eV. The time sliced velocity map images [8,53] of $CH_2^-$, $CH_3^-$, $CCN^-$ and $CHCN^-$ anions were measured at 8.0 and 8.3 eV incident electron energies and are shown in Fig. 5. Each of the images are of a 5-ns slice through the central part of the Newton sphere. The central sliced images of $CN^-$ and $CH_2CN^-$ for all the five different incident electron energies are shown in Fig. 6. The VMI images of $CN^-$ for 8.0 and 8.3 eV and of $CH_2CN^-$ for 3.3, 3.6 and 3.9 eV are of 1 ns width, and other images are of 5 ns width around the central part of the Newton sphere. The incident electron beam direction is along the positive x-axis through the centre of the each images and is indicated by the small red arrows.

Due to poor the mass resolution, the different mass fragments are not completely separated in the VMI spectrometer, especially $CCN^-$, $CHCN^-$ and $CH_2CN^-$ (38, 39 and 40-Da, respectively) are considerably overlapped, as can be seen in the mass spectrum of Fig. 2. However to obtain the central slice images only the ions with 1 or 5 ns time spread around the mass peak were considered. For the currently used spectrometer settings, around the 40 Da mass region a 5-ns time spread corresponds to around 0.08 Da mass spread. Therefore,

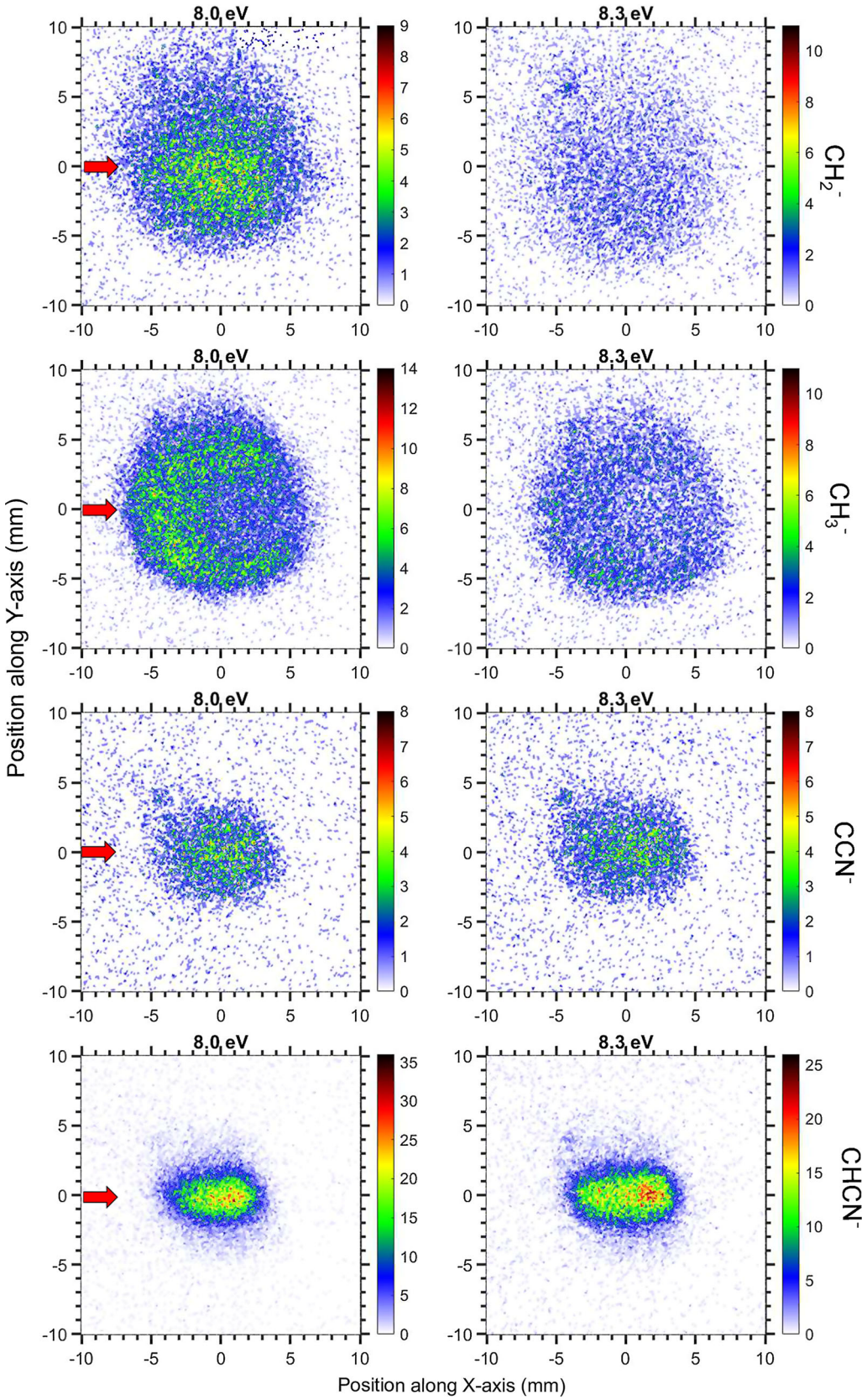


**Fig. 5** The velocity map images of $CH_2^-$, $CH_3^-$, $CCN^-$ and $CHCN^-$ for two different incident electron energies are shown in the successive four rows, respectively. The incident electron beam is along the positive x-axis through the centre of each images as indicated by the small red arrows

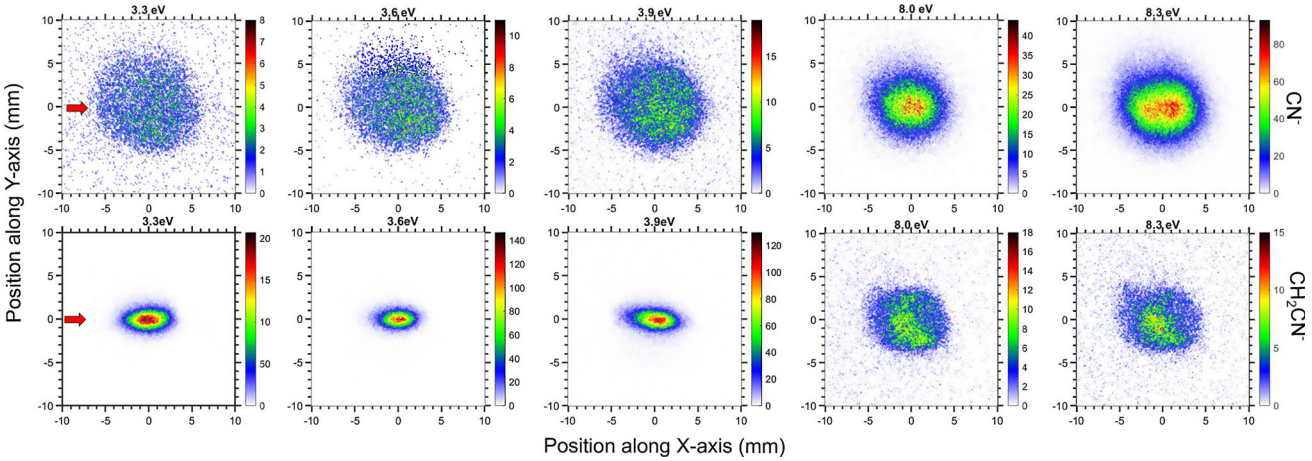


**Fig. 6** The velocity map images of $CN^-$ and $CH_2CN^-$ for five different incident electron energies are shown in the upper and lower panel, respectively. The incident electron beam is along the positive x-axis through the centre of each images as indicated by the small red arrows

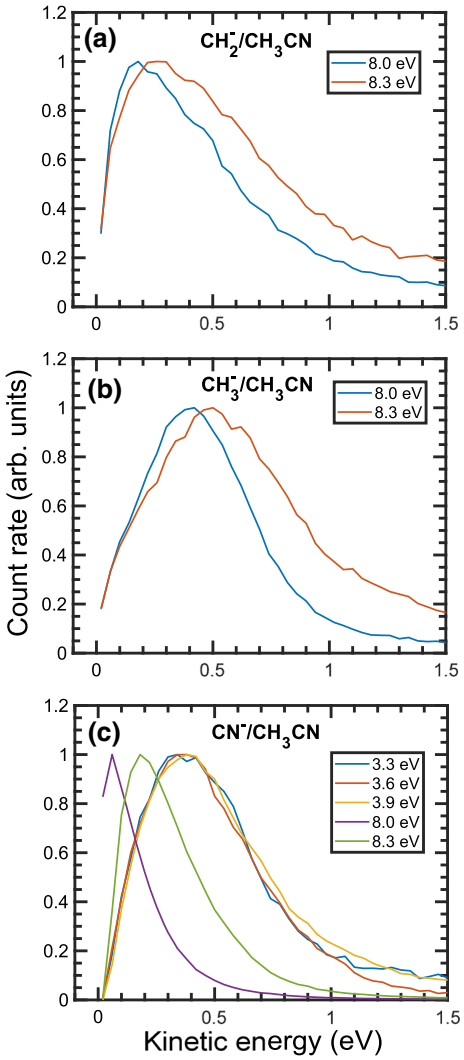


**Fig. 7** Kinetic energy distributions of the (a) $CH_2^-$, (b) $CH_3^-$ and (c) $CN^-$ ions produced for different incident electron energies, as indicated in the individual figures

in the time sliced images (Figs. 5 and 6) the contribution of any neighbouring mass is negligibly small.

## Kinetic energy distribution

The kinetic energy distributions of the $CH_2^-$, $CH_3^-$ and $CN^-$ anions measured considering all the ions produced within the entire Newton half sphere (see [7] for details) are shown in Fig. 7. For $CCN^-$, $CHCN^-$ and $CH_2CN^-$ mass fragments kinetic energy distribution measurement was not possible due to higher overlaps with the neighbouring masses. Nevertheless, only by looking at the central slice images of these fragment anions, it is possible to qualitatively assess the kinetic energy distribution pattern.

From the experiment, it is observed that for 3.3, 3.6 and 3.9 eV incident electron energies, the $CN^-$ ions are produced with a kinetic energy distribution that peaks at around 0.35 eV. Only the first reaction pathway mentioned in Table 2 ($CH_3CN^- \rightarrow CN^- + CH_3$) can lead to $CN^-$ formation around the low incident electron energy peak, whereas for 8.0 and 8.3 eV, the $CN^-$ ions are produced with kinetic energy distributions that peaks at around 0 and 0.15 eV, respectively, which suggests that most probably the three body breakup channels, as shown in Table 2, are involved. The two-body breakup channel, $CH_3CN^- \rightarrow CN^- + CH_3$, can only lead to DEA at 8.0 and 8.3 eV if the fragments are produced with a considerable amount of internal energy. In a recent study, Li et al. [29] measured the kinetic energy distribution of $CN^-$ fragments formed by electron attachment to acetonitrile at 7.1, 7.6 and 8.1 eV incident electron energies. For all the three incident electron energies, the kinetic energy distribution was reported to be very low. The reported kinetic energy peak position for 8.1 eV incident electron energy is similar to the currently measured kinetic energy distribution for 8.0 eV incident electron energy. But, in the present report, the width of kinetic energy distribution is much wider. This

**Table 2** The calculated maximum kinetic energy of $CN^-$ fragment produced for different incident electron energies via different reaction channels

| Dissociation channel | $E_{ke}$ of $CN^-$ (eV) | | | | |
|---|---|---|---|---|---|
| $E_{in}$= | 3.3 | 3.6 | 3.9 | 8.0 | 8.3 |
| $CN^- + CH_3$ | 0.8 | 0.9 | 1.0 | 2.5 | 2.6 |
| $CN^- + CH(d) + H_2$ | – | – | – | 0.8 | 0.9 |
| $CN^- + CH_2(t) + H$ | – | – | – | 0.8 | 0.9 |
| $CN^- + CH_2(s) + H$ | – | – | – | 0.6 | 0.7 |
| $CN^- + CH(q) + H_2$ | – | – | – | 0.5 | 0.6 |

The different reaction channels are listed on the left column and the kinetic energy for stated incident electron energies (in eV) are on the right

effect might arise due to the different data processing techniques used in the present report and by Li et al. to convert the pixel to kinetic energy. As discussed in earlier reports [7,42], kinetic energy obtained from the VMI images using flat slicing method always overestimates the ions produced at lower kinetic energies. In the present report, the entire half-'Newton sphere' has been considered in the calculation of the kinetic energy distribution of the ions and overcome the problem with flat slicing.

Qualitatively, the $CCN^-$ and $CHCN^-$ ions are also produced with low kinetic energy compared to that of $CH_2^-$ ions for the 8.0 and 8.3-eV incident electron energies. For 3.3, 3.6 and 3.9 eV incident electron energies, the $CH_2CN^-$ ions are produced with very narrow kinetic energy peak around 0 eV and do not appear to change with the incident electron energy. For 8.0 and 8.3 eV, $CH_2CN^-$ ions are produced with relatively higher kinetic energy but definitely lower than around 0.4 eV.

The threshold energy ($E_{th}$) for the production of all the seven observed anionic fragments via different reaction channels had been calculated and is listed in Table 1. Using the $E_{th}$ values, as defined in Eq. 4 and listed in Table 1, into Eq. 3, it is possible to calculate the maximum kinetic energy of each fragment. The calculated maximum kinetic energy for the production of $CH_2^-$ and $CH_3^-$ fragments with 8.0 and 8.3 eV incident electron energies are shown in Table 3. It is considered that the temporary negative ion dissociates via the paths $CH_3CN^- \rightarrow CH_2^- + HCN$ and $CH_3CN^- \rightarrow CH_3^- + CN$ to produce the $CH_2^-$ and $CH_3^-$ fragments, respectively. The neutral fragments are considered to be in the ground states. From the experiment for 8.0 and 8.3 eV electron energies, the $CH_2$ ions are found to be produced with a kinetic energy peak around 0.1 and 0.2 eV respectively, whereas the $CH_3^-$ ions are produced with kinetic energy peak around 0.4 and 0.5 eV for the two incident electron energies, respectively.

**Table 3** The calculated maximum kinetic energy of $CH_2^-$ and $CH_3^-$ fragments for two different incident electron energies, considering the neutral fragments are produced in ground state

| $E_{in}$ (eV) | $E_{ke}$ (eV) | |
|---|---|---|
| | $CH_2^-$ | $CH_3^-$ |
| 8.0 | 2.8 | 1.8 |
| 8.3 | 3.0 | 2.0 |

See text for detailed discussion

## Angular distribution

Time sliced velocity map images shown in Figs. 5 and 6 carry information about the angular distribution of the fragment negative ions. The statics for some of the ions is too low for complete quantitative analysis, but nevertheless, it is possible to qualitatively assess the images to determine if there is any significant angular distribution.

The $CH_2^-$ ions produced at 8.0 and 8.3 eV have an almost isotropic angular distribution. However, the $CH_3^-$ ions created due to 8.0 and 8.3 eV incident electron show a clear forward-backward asymmetry, where the ions are preferentially produced in the backward direction. The $CCN^-$ ions show no angular dependencies. The central sliced VMI of $CHCN^-$ ions at 8.0 and 8.3 eV appears to be a slightly elongated along the incident electron beam direction. However, this effect might be an experimental artefact. When the kinetic energy of the produced ion fragments are low, any non-homogeneous electric field or other experimental imperfection might lead to this kind of elongated structure.

To the best of our knowledge, only one previous report on the angular distribution of $CN^-$ ions around the 8.0 eV peak is available in the literature [29], showing primarily an isotropic distribution. The authors reported a small anisotropic distribution on top of the isotropic distribution. In the present experiment, at all five of the incident electron energies, the $CN^-$ angular distribution appears to be primarily isotropic. For 3.3, 3.6 and 3.9 eV incident electron energies, a slight forward-backward asymmetry, with ions preferentially produced in the forward direction, may be observed. However, the statistics are too low and the asymmetry, if present at all, is too small to conclude anything. For 8.0 and 8.3 eV, the ions appear to primarily form an isotropic distribution.

For 3.3, 3.6 and 3.9 eV incident electron energies, the $CH_2CN^-$ ions are produced with very low kinetic energy and the images appear to be isotropic. For 8.0 and 8.3 eV, the $CH_2CN^-$ ions are produced with a larger diameter, i.e. higher kinetic energies. The images appear to have a forward-backward asymmetry with fragments primarily appearing in the backward direction.

## 5 Conclusion

In conclusion, we studied the electron attachment to acetonitrile and acetonitrile-$d_3$ using three separate experimental setups. Consistent with previous measurements, the anion products $CH_3^-$, $CN^-$, $CCN^-$, $CHCN^-$ and $CH_2CN^-$ were observed, in addition to the products $D^-$ and $CH_2^-$, which were observed in the gas phase for the first time.

Detection of the $H^-$ fragment is hindered by the limitations of experimental setups as well as common $H^-$ backgrounds. Therefore, we used deuterated sample to confirm the presence of this reaction channel in DEA to acetonitrile. Measurements with the deuterated sample allow us to also show that the lifetime of parent acetonitrile ion $CH3CN^-$ is shorter than 4 $\mu$s, which is the time required for detection in the present experiments. We do not expect formation of stable valence bound anion for acetonitrile isolated in the gas phase.

We measured the ion yield curves for each product ion, where strong electron attachment was observed at incident electron energies of 3.5 eV and 8.0 eV. The ion yield curves reported here are mostly consistent with the previous measurements of Heni and Illenberger [21] and Sailer et al. [22], but have some differences with the measurements of Stockdale et al. [20] and Li et al. [29], particularly in the position of resonances for $CN^-$.

Velocity map images of the product ions $CH_2^-$, $CH_3^-$, $CN^-$, $CCN^-$, $CHCN^-$ and $CH_2CN^-$ were measured at different incident electron energies. From these images, we quantitatively measured the kinetic energy distribution of the $CH_2^-$, $CH_3^-$ and $CN^-$ ions, and qualitatively assessed the angular distributions. For 8.0 eV incident electron energy similar to Li *et al.*, we had observed the $CN^-$ ions having kinetic energy peak around zero eV, but our kinetic energy distribution has a different shape due to different evaluation procedure. In contrast to the report of Li et al., we were not able to observe any anisotropic angular distribution in the production of the $CN^-$ ion fragments.

**Acknowledgements** The authors acknowledge Dr Juraj Fedor for valuable suggestions and fruitful discussion throughout the entire stage of the present work. L.T. acknowledges the support from COST (European Cooperation in Science and Technology) Action CA18212 - Molecular Dynamics in the GAS phase (MD-GAS). The work has been supported by the Czech Science Foundation Project Nr. 20-11460S.

## Author contributions

TL measured performed the experiments with TEM-QMS setup and performed the quantum chemical calculations. JK and LT performed the experiments using CLUB setup. PN performed the experiments with the DEA-VMI setup. TL and PN prepared the manuscript. All the authors contributed to the final version of the manuscript and approved it.

**Data availability statement** This manuscript has no associated data or the data will not be deposited. [Authors' comment: All the data will be provided at reasonable request by the authors.]

## References

1. R.J. Habing, G.H. MacDonald, Astron. Astrophys. **252**, 705 (1991)
2. C. Watson, E. Churchwell, V. Pankonin, J.H. Bieging, Astrophys. J. **577**, 260 (2002)
3. A. Coustenis, B. Schmitt, R. Khanna, F. Trotta, Planet. Space Sci. **47**, 1305 (1999)
4. V. Vuitton, P. Lavvas, R. Yelle, M. Galand, A. Wellbrock, G. Lewis, A. Coates, J.E. Wahlund, Planet. Space Sci. **57**, 1558 (2009)
5. A. Brack, *The Molecular Origins of Life: Assembling Pieces of the Puzzle* (Cambridge University Press, Cambridge, 1998)
6. T.P.R. Kumar, P. Nag, M. Rankovic, R. Curik, A. Knížek, S. Civiš, M. Ferus, J. Trnka, K. Houfek, M. Cizek et al., Phys. Rev. A **102**, 062822 (2020)
7. P. Nag, M. Polášek, J. Fedor, Phys. Rev. A **99**, 052705 (2019)
8. P. Nag, D. Nandi, Phys. Chem. Chem. Phys. **17**, 7130 (2015)
9. Y. Kawarai, T. Weber, Y. Azuma, C. Winstead, V. McKoy, A. Belkacem, D. Slaughter, J. Phys. Chem. Lett. **5**, 3854 (2014)
10. B. Boudaïffa, P. Cloutier, D. Hunting, M.A. Huels, L. Sanche, Science **287**, 1658 (2000)
11. M. Mahmoodi-Darian, S. Tian, S. Denifl, S. Matejcik, T. Märk, P. Scheier, Int. J. Mass Spectrom. **293**, 51 (2010)
12. A.P. Hitchcock, M. Tronc, A. Modelli, J. Phys. Chem. **93**, 3068 (1989). https://doi.org/10.1021/j100345a039
13. P.D. Burrow, A.E. Howard, A.R. Johnston, K.D. Jordan, J. Phys. Chem. **96**, 7570 (1992). https://doi.org/10.1021/j100198a017
14. F. Edard, A.P. Hitchcock, M. Tronc, J. Phys. Chem. **94**, 2768 (1990). https://doi.org/10.1021/j100370a010
15. M. Gochel-Dupuis, J. Delwiche, M.J. Hubin-Franskin, J.E. Collin, F. Edard, M. Tronc, J. Am. Chem. Soc. **112**, 5425 (1990). https://doi.org/10.1021/ja00170a005
16. M.M. Fujimoto, E.V.R. de Lima, J. Tennyson, Eur. Phys. J. D **69**, 153 (2015)
17. G.L. Gutsev, A.L. Sobolewski, L. Adamowicz, Chem. Phys. **196**, 1 (1995)
18. P.R. Brooks, P.W. Harland, S.A. Harris, T. Kennair, C. Redden, J.F. Tate, J. Am. Chem. Soc. **129**, 15572 (2007)

19. R.J. Warmack, J.A.D. Stockdale, H.C. Schweinler, J. Chem. Phys. **72**, 5930 (1980). https://doi.org/10.1063/1.439091
20. J.A. Stockdale, F.J. Davis, R.N. Compton, C.E. Klots, J. Chem. Phys. **60**, 4279 (1974). https://doi.org/10.1063/1.1680900
21. M. Heni, E. Illenberger, Int. J. Mass Spectrom. Ion Process. **73**, 127 (1986)
22. W. Sailer, A. Pelc, P. Limão-Vieira, N. Mason, J. Limtrakul, P. Scheier, M. Probst, T. Märk, Chem. Phys. Lett. **381**, 216 (2003)
23. I. Ipolyi, W. Michaelis, P. Swiderek, Phys. Chem. Chem. Phys. **9**, 180 (2007)
24. A.D. Bass, J.H. Bredehöft, E. Böhler, L. Sanche, P. Swiderek, Eur. Phys. J. D **66**, 53 (2012)
25. T. Sugiura, A. Arakawa, Proceedings of the international conference on mass. Spectroscopy **72**, 848 (1970)
26. C.E. Klots, J. Chem. Phys. **62**, 741 (1975)
27. R. Hashemi, E. Illenberger, J. Phys. Chem. **95**, 6402 (1991). https://doi.org/10.1021/j100170a002
28. S. Tsuda, A. Yokohata, T. Umaba, Bull. Chem. Soc. Jpn. **43**, 3383 (1970)
29. H. Li, X.F. Gao, X. Meng, S.X. Tian, J. Phys. Chem. A **123**, 9089 (2019)
30. R. Janečková, D. Kubala, O. May, J. Fedor, M. Allan, Phys. Rev. Lett. **111**, 213201 (2013)
31. M. Zawadzki, T.F.M. Luxford, J. Kočišek, J. Phys. Chem. A **124**, 9427 (2020)
32. M. Stepanović, Y. Pariat, M. Allan, J. Chem. Phys. **110**, 11376 (1999). https://doi.org/10.1063/1.479078
33. J. Langer, M. Zawadzki, M. Fárník, J. Pinkas, J. Fedor, J. Kočišek, Eur. Phys. J. D **72**, 112 (2018)
34. M. Fárník, J. Fedor, J. Koçišek, J. Lengyel, E. Pluhařová, V. Poterya, A. Pysanenko, Phys. Chem. Chem. Phys. **23**, 3195 (2021)
35. M. Fárník, J. Lengyel, Mass Spectrom. Rev. **37**, 630 (2018)
36. M. Zawadzki, Eur. Phys. J. D **72**, 12 (2018). https://doi.org/10.1140/epjd/e2017-80540-8
37. M. Ranković, J. Chalabala, M. Zawadzki, J. Kočišek, P. Slavíček, J. Fedor, Phys. Chem. Chem. Phys. **21**, 16451 (2019)
38. J. Kočišek, K. Grygoryeva, J. Lengyel, M. Fárník, J. Fedor, Eur. Phys. J. D **70**, 98 (2016)
39. M. Ranković, T.P.R. Kumar, P. Nag, J. Kočišek, J. Fedor, J. Chem. Phys. **152**, 244304 (2020)
40. M. Allan, J. Electron Spectrosc. Relat. Phenom. **48**, 219 (1989)
41. J. Fedor, O. May, M. Allan, Phys. Rev. A **78**, 032701 (2008)
42. A. Moradmand, D.S. Slaughter, A.L. Landers, M. Fogle, Phys. Rev. A **88**, 022711 (2013)
43. R. Dressler, M. Allan, Chem. Phys. **92**, 449 (1985)
44. P. Nag, D. Nandi, Phys. Rev. A **91**, 052705 (2015)
45. M.J. Frisch, G.W. Trucks, H.B. Schlegel, G.E. Scuseria, M.A. Robb, J.R. Cheeseman, G. Scalmani, V. Barone, G.A. Petersson, H. Nakatsuji et al., *Gaussian-16 Revision C.01* (Gaussian Inc, Wallingford, 2016)
46. R. Janečková, O. May, J. Fedor, Phys. Rev. A **86**, 052702 (2012)
47. E. Fermi, E. Teller, Phys. Rev. **72**, 399 (1947)
48. W. Garrett, Chem. Phys. Lett. **5**, 393 (1970)
49. W.R. Garrett, J. Chem. Phys. **69**, 2621 (1978)
50. P. Alston Steiner, W. Gordy, J. Mol. Spectrosc. **21**, 291 (1966)
51. C. Desfrançois, H. Abdoul-Carime, C. Adjouri, N. Khelifa, J.P. Schermann, Europhys. Lett. (EPL) **26**, 25 (1994)
52. E. Illenberger, J. Momigny, *Gaseous Molecular Ions: An Introduction to Elementary Processes Induced by Ionization* (Steinkopff, Heidelberg, 1992)
53. D. Nandi, V.S. Prabhudesai, E. Krishnakumar, A. Chatterjee, Rev. Sci. Instrum. **76**, 053107 (8) (2005)